
Volume 277, Issues 3–4
30 January 2009
ISSN 0012-821X
ELSEVIER
EARTH
& PLANETARY
SCIENCE LETTERS
Editors
Rick Carlson, Washington, DC
Peggy Delaney, Santa Cruz, CA
Peter B. deMenocal, Palisades, NY
T. Mark Harrison, Los Angeles, CA
Tilman Spohn, Berlin
Lars Stixrude, London
Rob van der Hilst, Cambridge, MA
Frontiers Editor
Albrecht W. Hofmann, Mainz

Earth and Planetary Science Letters 277 (2009) 464–473

Contents lists available at ScienceDirect

Earth and Planetary Science Letters

journal homepage: www.elsevier.com/locate/epsl

Gravitational potential stresses and stress field of passive continental margins: Insights from the south-Norway shelf

Christophe Pascal [a,b,*], Sierd A.P.L. Cloetingh [b]

[a] NGU, Geological Survey of Norway, N-7491 Trondheim, Norway
[b] Faculty of Earth and Life Sciences, Vrije Universiteit, De Boelelaan 1085, 1081 HV Amsterdam, The Netherlands

ARTICLE INFO

Article history:
Received 17 June 2008
Received in revised form 11 November 2008
Accepted 12 November 2008
Available online 19 December 2008

Editor: T. Spohn

Keywords:
(neo)tectonics
topography
heat flow
lithosphere structure
seismicity

ABSTRACT

It is commonly assumed that the stress state at passive margins is mainly dominated by ridge push and that other stress sources have only a limited temporal and/or spatial influence. We show, by means of numerical modelling, that observed variations in lithosphere structure and elevation from a margin towards continental interiors may also produce significant gravitational potential stresses competing with those induced by ridge push forces. We test this hypothesis on an actual case where abundant geological and geophysical datasets are available, the shelf of southern Norway and adjacent southern Norwegian mountains (or Southern Scandes). The modelling results are consistent with the main features of three key-observables: (1) undulations of the truncated geoid (reflecting variations in gravitational potential energy in the lithosphere), (2) significant stress rotations both offshore and onshore and (3) the seismicity pattern of southern Norway. The contribution of the Southern Scandes to the regional stress pattern appears to be far more significant than previously anticipated. In addition, the modelling provides a physical explanation for the enigmatic seismicity of southern Norway. Gravitational potential stresses arising from variations in the lithospheric structure between a passive margin and its continental borderlands, can exert a significant control on the dynamic evolution of the margin in concert with ridge push.

1. Introduction

It is commonly accepted that the main stress source affecting passive margins is ridge push and that other stress sources (e.g. flexural loading by rapid sedimentation rates, post-glacial rebound) have only local and/or short-term significance (Stein et al., 1989). This statement finds support in the numerous stress directions measured at passive margins that, in general, show maximum horizontal compression perpendicular to mid-oceanic ridges (Heidbach et al., 2008). Ridge push forces are, by nature, forces taking their origin in the excess of gravitational potential energy (hereafter GPE) existing between mid-oceanic ridges and most of the Earth's lithosphere and, in particular, oceanic basins and continental margins (Dahlen, 1981). GPE is directly linked to the elevation and the density structure through depth of a given lithospheric column (Artyushkov, 1973). Mid-oceanic ridges present higher levels in potential energy with respect to passive margins, because the mantle stands at a higher position in the former case than in the latter. Pronounced differences in structure (i.e. elevation, Moho depth and crust and mantle density) also exist between continental margins and interiors. These differences are expected to result in significant gravitational stresses (Fig. 1). Their involvement in quantitative studies appears to be a requirement to fully understand the stress state at passive margins.

In the present paper, we compute lithospheric stresses induced by ridge push forces and continental elevation at passive margins. The numerical method used accounts for the thermal and density structure of the lithosphere (Pascal, 2006) and is briefly described in the first section. In the second section, we show results from synthetic models and explore their sensitivity as a function of topography and crustal thickness variations. Finally, we apply the method to the shelf areas of southern Norway and consider various geophysical datasets (i.e. geoid, stress measurements and seismicity) to discuss the modelling results.

2. Methodology

We briefly summarise here the main principles of the numerical method used to compute GPE and gravitational potential stresses (hereafter GPSt). An extensive description of the method can be found Pascal (2006). The numerical method involves classical steady-state heat equations to derive lithosphere thickness, geotherm and density distribution and, in addition, requires the studied lithosphere to be isostatically compensated at its base. The density of the crust is fixed a priori whereas mantle lithosphere densities are calculated as a function of temperature and pressure. Local isostatic equilibrium is calculated with respect to an ideal reference asthenosphere column

* Corresponding author. NGU, Geological Survey of Norway, N-7491 Trondheim, Norway. Fax: +47 73904494.
E-mail address: christophe.pascal@ngu.no (C. Pascal).

0012-821X/$ – see front matter © 2008 Elsevier B.V. All rights reserved.
doi:10.1016/j.epsl.2008.11.014

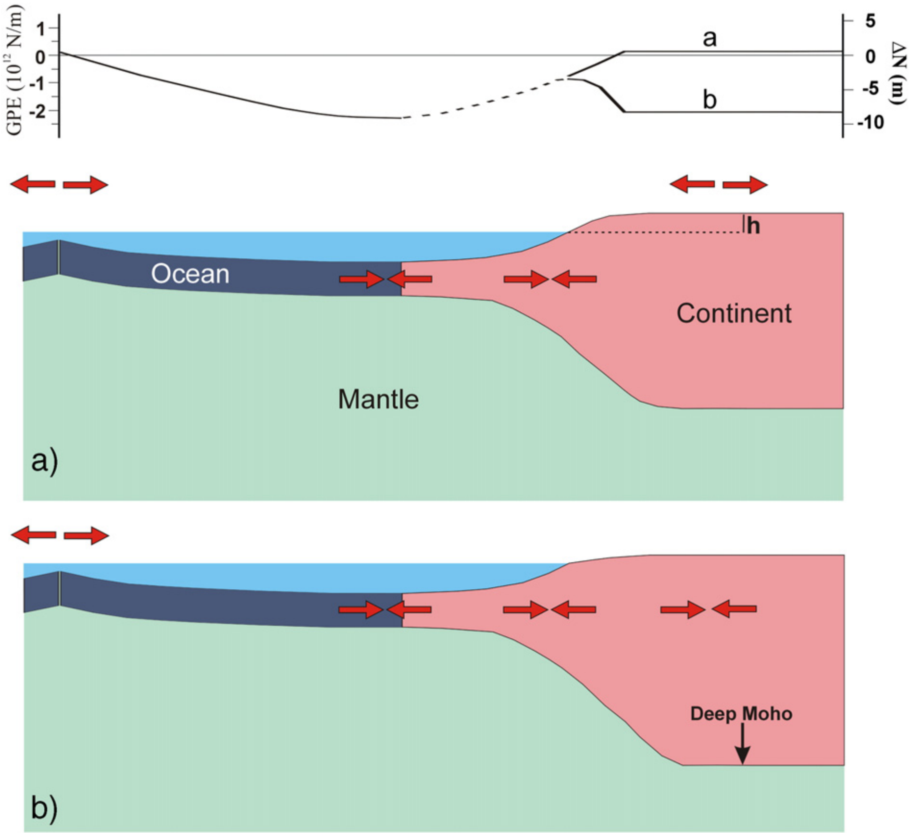

Fig. 1. Cartoon illustrating how gravitational stresses affect a passive continental margin. The upper panel shows the variation in gravitational potential energy (GPE) and its associated geoid undulations. a) Continental landmasses are elevated and their GPE level exceeds GPE values at mid-oceanic ridges: the continent is under extension and adds a lateral compressive force on its passive margins. b) Continental landmasses are characterised by thick crust and subdued topography: ridge push forces dominate both onland and offshore.

(Lachenbruch and Morgan, 1990). The density structure of the reference column is computed according to its average composition and depth-dependent P–T conditions.

For each computed geotherm, the condition for local isostasy is tested against the condition that the reference density for mantle lithosphere ranges between 3300 and 3390 kg/m^3, in agreement with density values derived from petrologic studies of mantle xenoliths (Boyd and McCallister, 1976; Jordan, 1988; Boyd, 1989; Boyd et al., 1999; Poudjom Djomani et al., 2001; James et al., 2004). The procedure described above allows for excluding numerically geotherms or conversely density structures that, in the case of reasonable mantle density values, would result in out-of-balance isostatic states. An additional condition is added: the base lithosphere depth has to remain in between Moho depth and the peridotite–spinel transition phase at 410 km depth.

Once the thermal structure, the thickness and the density structure of the lithosphere are determined, it is possible to compute GPE and subsequent GPSt for this lithospheric column. Gravitational potential energy and stresses are the result of contrasting density distributions between the studied lithosphere column and the reference column (e.g. Artyushkov, 1973; Fleitout and Froidevaux, 1982; Coblentz et al., 1994). The difference in GPE, ΔGPE, is linked to the respective density distributions inside the two columns through:

$$\Delta\text{GPE} = \int_h^{Z_{\text{bl}}} \left(\sigma_{zz}(z) - \sigma_{zz}^{\text{R}}(z)\right) dz \tag{1}$$

where h is elevation with the convention that negative values correspond to surface above sea-level, z_{bl} base lithosphere depth and $\sigma_{zz}(z)$ and $\sigma_{zz}^{\text{R}}(z)$ are lithostatic pressures for the lithospheric and reference columns respectively.

Potential stresses are written as a function of the elastic thickness of the lithosphere, T_e, and

$$\text{GPSt} = \frac{\Delta\text{GPE}}{T_e} \tag{2}$$

meaning that only those parts of the lithosphere that do not yield at characteristic geological time scales support the applied stresses. T_e values are derived from the calculated lithospheric thermal and subsequent rheological structures, using the analytical formulae introduced by (McNutt et al. (1988) and Burov and Diament (1995).

3. Synthetic models: impact of varying surface topography and crustal thickness on the stress state at passive margins

Using the method described in the previous section, we computed GPE values for different configurations in terms of surface elevation and Moho depth for passive margins and adjacent continents. For the purpose of this study, we kept constant crustal density (i.e. ρ_c = 2800 kg/m^3) and surface heat flow (q_s = 60 mW/m^2) and assumed isostatic equilibrium and no tectonic perturbations of any kind. By nature, a passive margin is a transitional zone between deep oceanic basins and continental interiors, segmented in distinct areas presenting contrasting bathymetries and Moho depths. Therefore, it is, in general, inadequate to resume the crustal structure of a given passive margin by averaged bathymetry, Moho depth and crustal density values, and each margin, and eventually, each segment of the margin, needs to be treated separately. Nevertheless, our systematic exploration of the parameter space allows us to compute the a priori range of GPE values relevant for passive margins and more importantly, allows

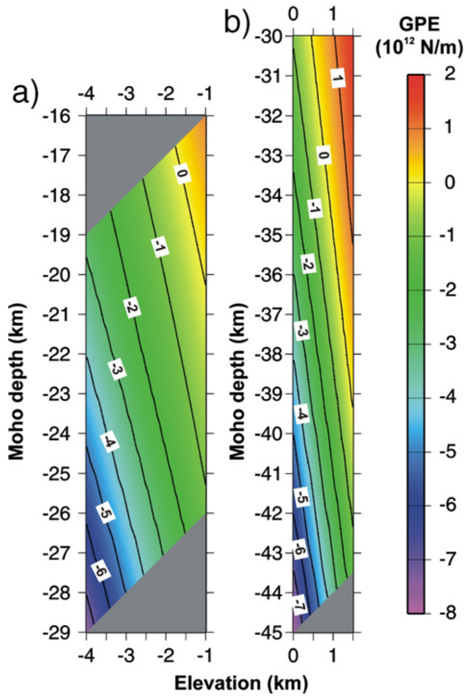

Fig. 2. Variation of gravitational potential energy (GPE) in function of surface elevation and Moho depth (negative values below sea-level) for a) passive margins and b) continental borderlands. Crustal density and surface heat flow are kept constant: ρ_c=2800 kg/m^3, q_s=60 mW/m^2. Positive GPE values result in extensional stresses.

us to estimate the range of ΔGPE that might exist between passive margins and adjacent continents.

The results of the modelling suggest that GPE values for passive margins can vary from -7×10^{12} to ~0 N/m depending on crustal thickness and elevation (Fig. 2a). Because the GPE state of our selected reference column does not differ significantly from the one associated to most mid-oceanic ridges (Pascal, 2006), the GPE values computed here can be directly taken as estimates of the net ridge push force. It should be noted that combinations of very shallow bathymetry with shallow Moho or deep bathymetry with thick crust are not very likely to occur in nature once isostatic equilibrium has been reached and, at least, for our selected ρ_c and q_s values. This suggests that realistic GPE values for passive margins should be in the middle of the plot in Fig. 2a (i.e. $-2\times10^{12}\pm1\times10^{12}$ N/m), in good agreement with the range of values proposed by e.g. Bott (1991). Note that the values devised here are first-order approximations that are expected to apply in most cases, where the geometrical configuration of the passive margin with respect to mid-oceanic ridges is relatively simple, but complex geometries would require more rigorous 3D calculations as pointed out by Ghosh et al. (2006).

The predicted range of GPE values for the adjacent continents is slightly broader than that modelled for passive margins (compare Fig. 2a with 2b) and eventually exceeds a level of 1×10^{12} N/m. GPE values increase with elevation but also decrease with Moho depth. It is interesting to note that the increase in GPE due to topography can be reduced and even cancelled out when the Moho deepens (e.g. Jones et al., 1996; Pascal, 2006). In brief, it is impossible to derive reliable GPE values from topography alone and more complete information on the crust/lithosphere structure is essential. We emphasise that the results shown in Fig. 2 are very sensitive to crustal density and refer to Pascal (2006) for a more complete exploration of the other input parameters, including heat flow. The major conclusion that can be drawn at this stage, is that even moderately elevated continents can eventually present GPE values exceeding those traditionally associated to mid-oceanic ridges and, therefore, can exert forces on their adjacent passive margins that reach or even overcome ridge push forces. For example, if continent and margin GPE values are equal to 1×10^{12} and -2×10^{12} N/m respectively, the net force applied to the margin by the "spreading tendency" of continental topography would be about -3×10^{12} N/m. Thus the stress state of passive margins bordered by elevated continents may be significantly disturbed. Note that stresses eventually originating from continental elevation are not always easy to detect using stress orientation data. This is because in most cases continent topography by passive margins stands parallel to the mid-oceanic ridges and, consequently, topographic and ridge-push stresses are parallel. In the following, we study an actual case where continental topography is anticipated to produce a detectable stress signal.

4. Application to a natural laboratory: the "south-Norway shelf"

We selected the shelf of southern Norway (i.e. southernmost Norwegian Margin and northern North Sea, hereafter referred to as south-Norway shelf) and adjacent areas as case study. Our choice was motivated by the presence of relatively high topography on land near the shelf (i.e. the Southern Scandes with peaks up to 2.5 km high, Fig. 3) and the wealth of offshore data whose quantity has been boosted by forty years of oil exploration. We used three input data sets (i.e. topography, Moho depth and heat flow, Fig. 4). Topography was extracted from the Etopo2 DEM and Moho depth is from Kinck et al. (1993). Both grids were high-pass filtered with a cutting wavelength at 300 km so that the remaining long-wavelength features were in agreement with local isostatic compensation and negligible lateral heat transport. Heat flow was taken from Pollack et al. (1993). Although this latter dataset is relatively coarse, the heat flow values give a first order picture of the regional heat flow distribution in reasonable agreement with unpublished data from the Geological Survey of Norway. Finally, in absence of firm constraints from seismic data in particular onshore, we used the empirical law established by Zoback and Mooney (2003) to derive densities of the crust according to its thickness (Fig. 4d).

The first modelling result is a map of the depth to the base lithosphere (i.e. 1300 °C isotherm) in the area under consideration here (Fig. 5a). Comparison with independent determinations from surface wave studies (Calcagnile, 1982) reveals that: (1) the modelled depth values are in agreement with those determined from seismic experiments and (2) a similar trend of eastward lithosphere thickening is predicted both by our modelling and the seismic model. Note that this trend has also been inferred from previous numerical modelling work (Pascal et al., 2004) and confirmed by recent passive seismic studies (Balling et al., 2006). In detail, the seismic study from Calcagnile (1982) predicts a much smoother pattern for the base of the lithosphere (Fig. 5b). This is, probably, because this latter study, conducted at the scale of Fennoscandia, had not enough resolution to resolve shorter wavelength features.

The computed GPE is shown in Fig. 6 together with the geoid truncated at degree and order 12 (i.e. at wavelengths associated to signals from lithospheric sources, Bowin, 1991). The main features of the truncated geoid reflect GPE variations in the lithosphere (e.g. Jones et al., 1996; Turcotte and Schubert, 2002) and can be used as a modelling constraint. At the first order, the modelled GPE distribution mimics well observed geoid undulations. The simulated GPE maximum of the Southern Scandes finds its actual counterpart in the pronounced positive geoid anomaly associated with the mountain range. In detail, some of the short-wavelength (i.e. less than ~100 km) geoid undulations are not well reflected in the modelled GPE distribution. These local mismatches are mainly due to the filtered and simplified crustal structure used in the modelling. For example, the deep Møre Basin, located at 4°E 64°N, produces a significant low in the geoid because the density of the sediments it hosts is significantly lower than basement densities. It is, however, important to note that the masses creating the short-wavelength signals are compensated by

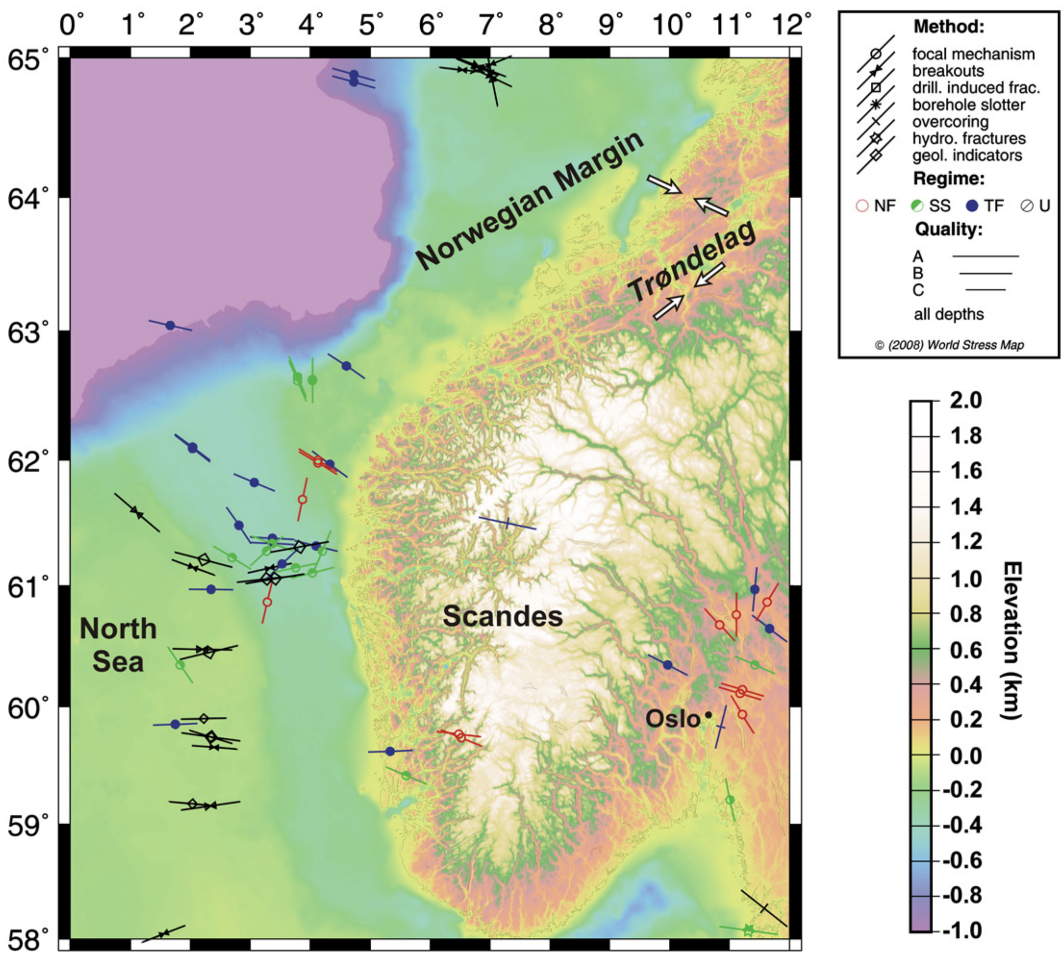

Fig. 3. Topography of southern Norway and adjacent areas and measured stress directions. Note the pronounced stress rotations in the northern North Sea and in Trøndelag. Stress data are from the World Stress Map (Heidbach et al., 2008). Stress orientations in Trøndelag are from Roberts and Myrvang (2004), double arrows represent compression.

flexural isostasy and cannot be reasonably addressed by the method used here. In turn, our discussion focuses on the long-wavelength signals (i.e. 100s of kms). A closer look at the predicted GPE pattern reveals that the excess in potential energy of the Southern Scandes (i.e. 0.4 to 0.6×10^{12} N/m) with respect to the surrounding basins (i.e. the Norwegian Margin to the north and the North Sea to the west with average GPE values from -1.2 to -0.8×10^{12} N/m) results in a net compressive force on the basins in between -1.8 to -1.2×10^{12} N/m.

We computed GPSt values according to Eq. (2). The T_e distribution (Fig. 7) needed for the GPSt calculation was derived from the modelled lithospheric thermal structure and the assumed rheology (Table 1). T_e values range in between ~20 and 35 km in the continent and remain in good agreement with previous estimates based on post-glacial rebound modelling (Fjeldskaar, 1997) and spectral methods (Rohrman et al., 2002; Pérez-Gussinyé and Watts, 2005) onshore and basin modelling offshore (ter Voorde et al., 2000). As expected predicted T_e values increase towards oceanic lithosphere (i.e. NW corner of the modelled domain, Fig. 7) but reach values up 50 km which appear to be overestimated for ~54 Ma old oceanic lithosphere (Watts et al., 1980). Nevertheless, this has no consequence on the results outside this specific domain which is not the prime target of the study.

As a final step in the modelling process, we imported the computed GPSt values in a finite-element model in order to quantify how the calculated stresses are distributed in a continuous medium. We used the commercial finite-element code ANSYS and proceeded in a similar manner as Bada et al. (2001), Andeweg (2002) and Jarosiński et al. (2006). The 2D model is purely elastic with constant Young's modulus and Poisson's ratio values (Table 1). Because the imported GPSt values are computed as a function of T_e, information on rheological variations in the modelled domain is already provided to the finite-element mesh when importing stress values and there is no need for further adjustments of its elastic parameters. This procedure remains physically consistent as long as we focus on modelling stresses. Fig. 8a depicts the predicted stress directions resulting from the previously calculated GPE and T_e values (Figs. 6 and 7). The excess in GPE associated to the Southern Scandes results in moderate extensional stresses at the location of the mountain range and a radial compression with respect to it. The modelled counterclockwise stress rotation from the Norwegian Margin to the North Sea is remarkably well supported by stress measurements (Fig. 3). In addition, recent stress measurements in southern Trøndelag mid-Norway (Fig. 3) demonstrate that the horizontal maximum compressive stress trends NE–SW and rotates NW–SE to the north in perfect agreement with our modelling results (Fig. 8a). Inversion of focal mechanisms of earthquakes from the western edge of the Southern Scandes suggest normal stress regimes (Hicks et al., 2000 and Fig. 8) and add again support to the validity of our approach.

Fig. 8b depicts modelled Von Mises Equivalent Stresses (hereafter VMES) together with seismicity (Dehls et al., 2000). The VMES is a scalar calculated from the stress tensor and can be used as a priori indicator for plastic yielding (e.g. Jaeger and Cook, 1969), brittle failure being more expected where high VMES values prevail. The use of such an indicator that ignores the contribution of hydrostatic stresses is here justified by our thin plate approach. The most seismically active areas in the modelled domain are the Jurassic Viking Graben in the

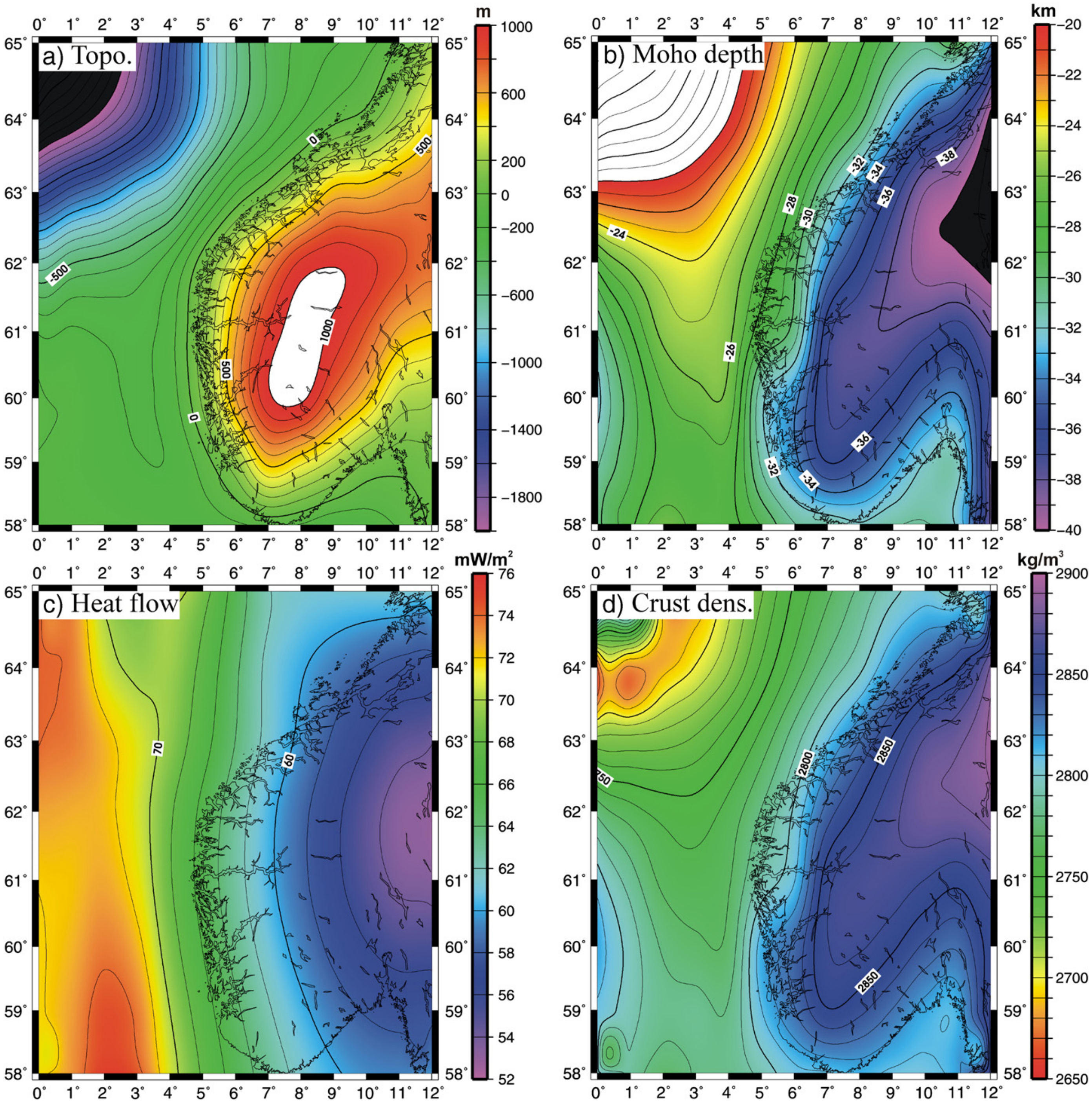

Fig. 4. Input data used in the modelling: a) topography, b) Moho depth and c) surface heat flow. The topography and Moho grids have been high-pass filtered using a cutting wavelength of 300 km. d) Assumed crust densities according to Zoback and Mooney (2003) (see text).

North Sea, the western and southern coasts of southern Norway and to some extent the Permian Oslo Graben (Hicks et al., 2000). The most remarkable result consists in predicting low VMES values by the centre of southern Norway, which is actually seismically quiet. VMES increase dramatically towards the western and southern coastlines, that are amongst the most seismically active regions onshore northern Europe (e.g. Bungum et al., 1991; Cloetingh et al., 2007). Obviously, the VMES pattern is strongly controlled by the interplay between the Atlantic ridge push and gravitational stresses related to the Southern Scandes. The results in Fig. 8a show an area of moderate extension at the centre of the mountain range, bordered by areas where the extensional stresses and ridge push cancel out mutually (i.e. corresponding to the low VMES areas in Fig. 8b). In contrast, the two stress sources appear to act in concert to enhance stress anisotropy, stress rotations and tendency for brittle failure by the coastline. Although we have some reservations about the robustness of our results in that specific area (because of artefacts related to model boundaries), our modelling appears also successful in predicting low VMES values close to the continent–ocean boundary in the NW. However, our modelling fails to give an explanation for the high

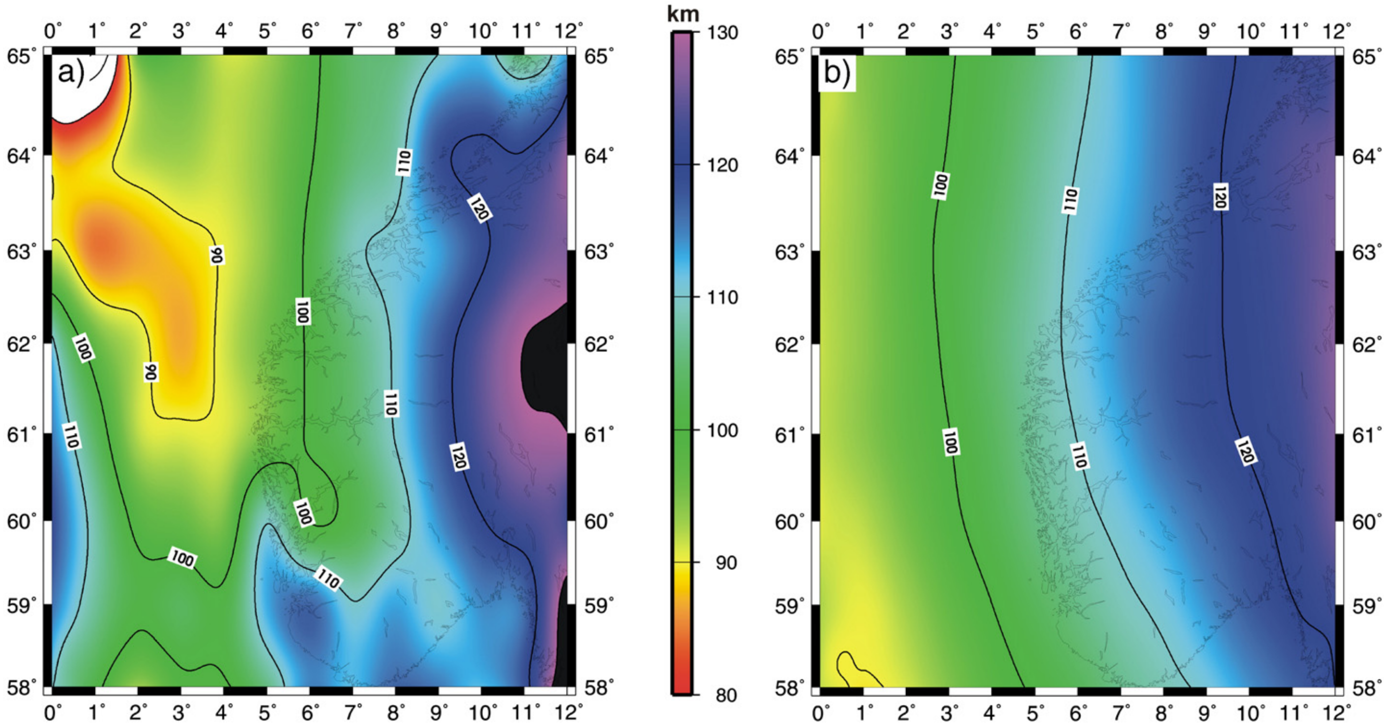

Fig. 5. a) Modelled depths for the base of the lithosphere, b) lithosphere thickness from surface wave studies (Calcagnile, 1982).

seismicity of the Viking and Oslo Grabens. This is not surprising because these rift structures are too narrow to be accounted for by the method used here, where small-scale features are filtered out from the input data in order to satisfy the background modelling hypotheses. More striking is the modelling of relatively high VMES values offshore Trøndelag that are not reflected in the seismicity. This is most probably related to a local overestimation in absolute GPE values, as suggested by the comparison between geoid undulations and modelled GPE (Fig. 6), but does not affect our predictions on the stress directions, that are, furthermore, confirmed by stress measurements (Roberts and Myrvang, 2004).

5. Discussion and concluding remarks

The modelling results presented here are mainly sensitive to variations in topography, Moho depth and crustal density. Heat flow influences notably GPE calculations only if it reaches typical low "cratonic" levels (i.e. ~40 mW/m^2) and leads to thick lithospheres

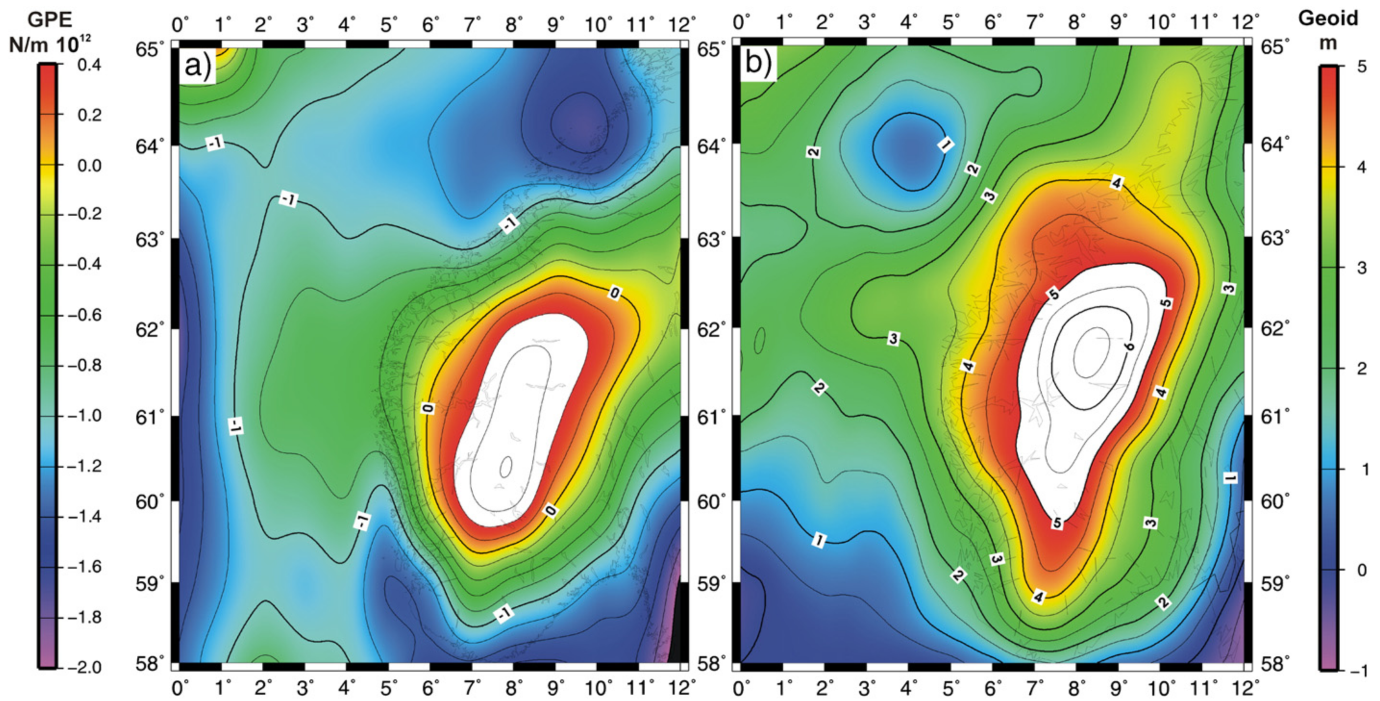

Fig. 6. a) Modelled potential energy, b) truncated geoid at degree and order 12 (EGM96 geoid model by Lemoine et al., 1996).

Table 1
Parameters used in this study

Quantity	Symbol	Value
Surface temperature	T_S	0 °C
Characteristic thickness	D	5 and 10 km
Max. crustal heat production	A_D	Computed
Heat flow ratio	R_q	Computed
Min. crustal heat production	A_{cmin}	0.3 μW/m^3
Crust thermal conductivity	k_C	2 W/m/K
Water density	ρ_W	1030 kg/m^3
Continental crustal density	ρ_C	Variable
Oceanic crustal density	ρ_{OC}	2850 kg/m^3
Base lithosphere temperature	T_{bl}	1300 °C
Mantle lithosphere heat production	A_M	0.01 μW/m^3
Mantle lithosphere thermal conductivity	k_M	4 W/m/K
Thermal expansion	α	Temp.-dependent K^{-1}
Mantle lithosphere compressibility	β_L	7.64 GPa^{-1}
Mantle lithosphere ref. density	ρ_{MRef}	3300–3390 (computed)
Buoyant height of sea-level	H_0	2500 m
Asthenosphere potential temperature	T_P	1300 °C
Mantle adiabat	F	0.5 °C/km
Asthenosphere compressibility	β_A	6.651 GPa^{-1}
Asthenosphere ref. density	ρ_{ARef}	3390 kg/m^3
Acceleration of gravity	g	10 m/s^2
Gravitational constant	G	6.67×10^{-11} Nm^2/kg^2
Friction coefficient[a]	μ	0.6
Pore pressure ratio	λ	0.35
Strain rate	ε'	10^{-15} s^{-1}

[a] Viscous creep is also modelled using dry granite (Carter and Tsenn, 1987) and dry olivine-dominated (Goetze and Evans, 1979) rheologies for the crust and the mantle respectively. FE model: Young's modulus and Poisson ratio are fixed to 80 GPa and 0.25 respectively.

(Pascal, 2006), which is definitively not the case in the area studied here (Calcagnile, 1982; Plomerová et al., 2001). The Moho has been well imaged by previous seismic experiments (Kinck et al., 1993 and references therein) and is not considered here to be a major source of errors. Furthermore, recent receiver function studies support the first order features of the Moho map of southern Norway (Svenningsen et al., 2007). However, because the old seismic experiments have been unable to furnish a clear image of the crust onshore, it is difficult to give a clear assessment on the validity of the input crustal density model we used here. The inferred variation in crustal densities (i.e. density increase from the sedimentary basins towards shield interiors, Fig. 4d) seems at the first order a reasonable assumption (Christensen and Mooney, 1995). The apparent good quality of the modelling results, and in particular the close similarity between the simulated GPE pattern and undulations of the truncated geoid, seems, however, to be dictated by the best-constrained input parameter that is topography and to some extent by Moho topography. This observation strongly suggests that the results are not, in the present case, very sensitive to lateral density changes in the crust. Recent and on-going active and passive seismic soundings onshore southern Norway will allow for refinements of our model in the near future.

Our GPE calculations are based on a simple 1D approach that has been proved to be in good agreement with more complete 2D ones (Bott, 1991). For the Indian Plate, Gosh et al. (2006) showed that GPE values calculated using a spherical thin-sheet model are reduced by half with respect to GPE values predicted by 2D models. However, our studied case is much simpler from the geometrical point of view than the Indian Plate case modelled by Ghosh et al. (2006). For example, mid-oceanic ridges show constant orientations in the northern Atlantic, allowing for 2D or 1D approaches. We recognise nevertheless that our results need to be confirmed by more advanced modelling methods but anticipate that our main findings will remain.

Despite artefacts at the edges of the model, our simulated stress pattern reflects in general the observed stress rotations (compare Fig. 8 with Fig. 3). In particular the counterclockwise rotation in the northern North Sea is remarkably well reproduced. This rotation has already been noticed (Bungum et al., 1991) and ascribed either to diverging ridge push directions in the NE Atlantic (Lindholm et al., 2000), deviation of far-field stresses caused by pre-existing major weak faults (Pascal and Gabrielsen, 2001) or post-glacial rebound flexural stresses (Grollimund and Zoback, 2000, 2003). To our opinion, the small-scale character of the stress rotation implies a local origin and is unlikely to result from far-field causes. Pre-existing discontinuities in the crust are prone to deviate far-field stresses (Gölke et al., 1996; Pascal and Gabrielsen, 2001). This effect is merely limited to areas in the close vicinity of the discontinuity in contrast with model predictions by Pascal and Gabrielsen (2001). We base this conclusion on the notion that the E–W trend for the maximum horizontal stresses appears to persist across domains with different structural grains in the North Sea and onshore Norway (Fig. 3). However, we acknowledge that in the N–S Viking Graben this E–W trend might be locally influenced by the boundary faults of the rift structure.

Alteration of the tectonic stress field by post-glacial rebound stresses stands as a natural explanation in Fennoscandia, formerly covered by an ice cap until ~10 kyr ago, and has been very often invoked in the literature (e.g. Stein et al., 1989; Fejerskov and Lindholm, 2000; Muir Wood, 2000). It is clear from the presence of impressive late glacial reverse faults in northern Fennoscandia (Olesen, 1988; Lagerbäck, 1990) that, in the past, the stress field has been significantly influenced by glacial unloading. However, as pointed out by Pascal et al. (2005) and Gregersen (2006), indicators of present-day stresses from formerly glaciated regions are mainly consistent with plate tectonic driving forces and no clear correlation with post-glacial rebound patterns can be seen (Heidbach et al., 2008). In case of significant post-glacial rebound stresses, it would be extremely doubtful that the area studied here would be the only one where a post-glacial stress signal could be detected.

Furthermore, in order to create significant flexural stresses, Grollimund and Zoback (2000, 2003) needed to assume ice thickness of more than 1 km over the mountains of southern Norway for most of the Pleistocene. To date, no consensus exists concerning the thickness of the ice that covered the Norwegian mountains during the last Ice Age (e.g. Winguth et al., 2005). Geomorphological studies (Nesje et al., 1988), cosmogenic nuclide datings (Brook et al., 1996) and ice-flow modelling (Winguth et al., 2005) tend to support a thin ice model in

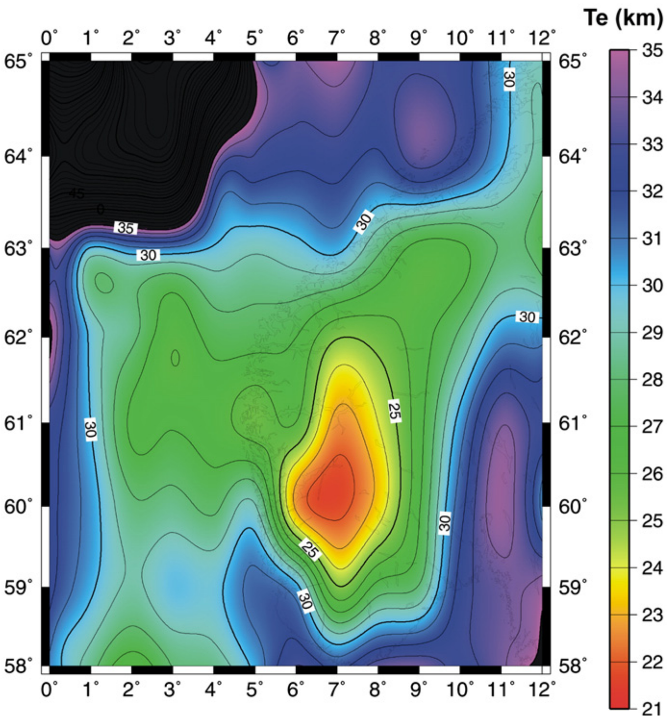

Fig. 7. Modelled elastic thickness (T_e) distribution.

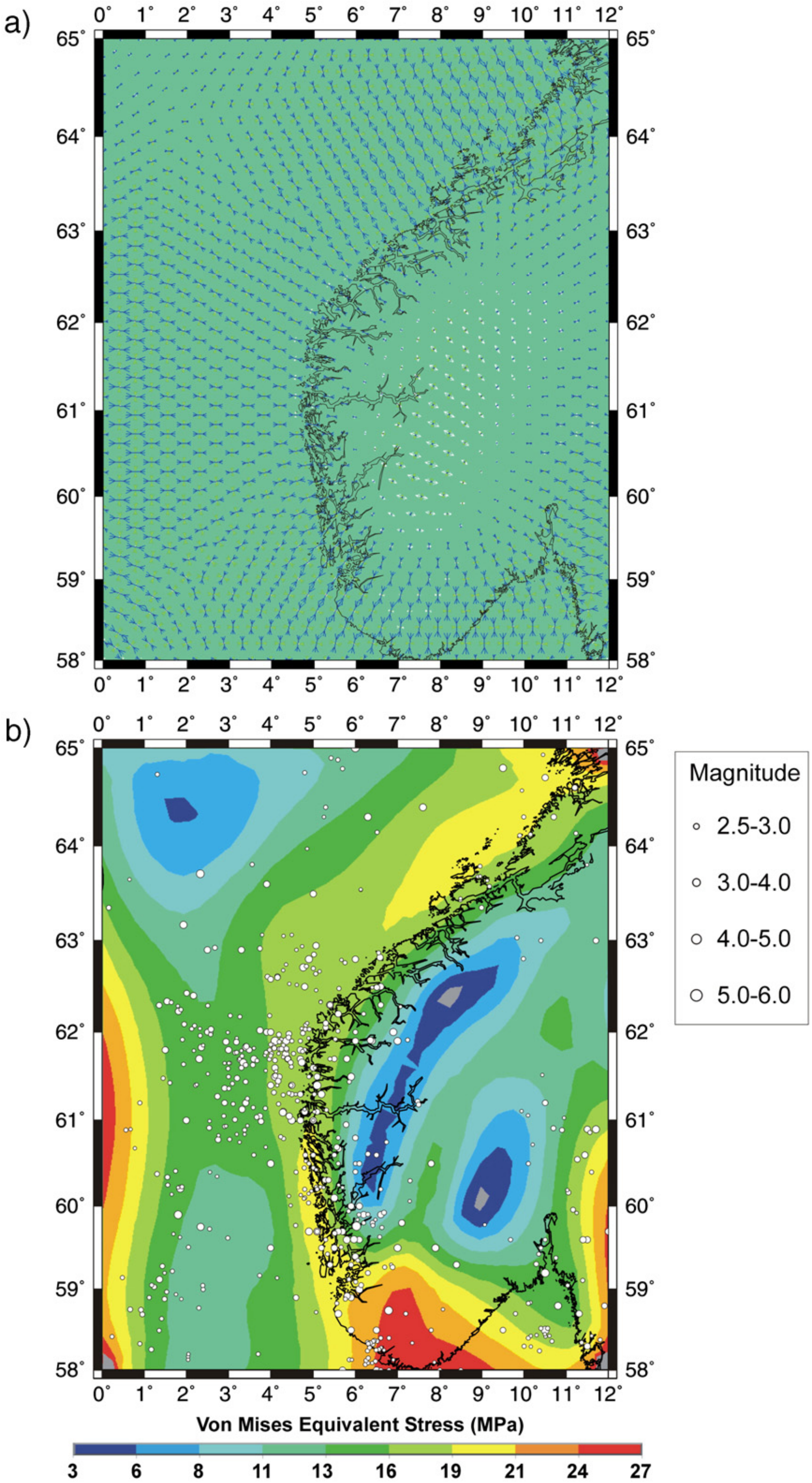

Fig. 8. Finite-element modelling of a) stress orientations and regimes (diverging arrows depict normal stress regimes, i.e. vertical maximum principal stresses) and b) Von Mises Equivalent Stresses. Seismicity from Dehls et al. (2000).

opposition with the modelling assumptions of Grollimund and Zoback (2000, 2003).

We should emphasize that the Southern Scandes are in excess of GPE with respect to the surroundings, as intuitively suggested by e.g. Lindholm et al. (1995). This is clearly proven by the geoid signal (Fig. 6). Other elements that add support to the validity of our model are: (1) its capacity to reproduce the stress rotation observed onshore in the Trøndelag region (Figs. 3 and 8a), not accounted for by previous models, and (2) the good agreement (at least onshore) between observed earthquake distribution and predicted areas for maximum brittle deformation (Fig. 8b).

Our study has obvious implications for other passive margins worldwide and eventually other settings. We showed here that a moderately elevated landmass can produce stresses competing with far-field induced stresses. This suggests that not only the system of mid-oceanic spreading ridges has to be considered when studying the dynamical evolution of a specific margin but also the spatial and temporal variations of adjacent continental topography. As a point of interest, many margins have been affected by post-breakup inversion. The debate on the causes of the inversion has been going on for several years (e.g. Bott, 1991; Doré et al., 2008). Our work suggests that uplift of the adjacent continents might, in some cases, furnish stresses with sufficiently high magnitudes capable of producing the observed inverted structures. Because the timing of uplift of the Scandes is not sufficiently well constrained (Rohrman et al., 2002), it is difficult, at the present stage, to judge on their potential influence on the development of the inverted structures present offshore Norway.

It is also tempting to speculate on the role of continental uplift on plate scale processes. Recent numerical modelling by Iaffaldano et al. (2006) suggests that buoyancy forces created by the recent uplift of the Andes could have slowed down convergence between the Nazca and South America plates. Similarly, the Cenozoic uplift of Scandinavia and Greenland might have contributed to the observed decrease of spreading rates of NE Atlantic ridges since Eocene times (Mosar et al., 2002).

Acknowledgements

The present work has been initially supported by NWO in the framework of the ESF Eurocores/Euromargins Programme (Nemsdyn-EMA16 Project). C. Pascal benefited from a visiting research fellowship from the Netherlands Research Centre for Integrated Solid Earth Science (ISES NedSeis-2.7) to finalise the present Ms. We are indebted to Fred Beekman (VU Amsterdam) for providing help while using Ansys. Bernhard Steinberger (NGU) is kindly acknowledged for his help with the geoid data. We thank two anonymous reviewers for very accurate and thoughtful reviews. This is the Netherlands Research School of Sedimentary Geology (NSG) publication nr. 2008.09.01. Maps have been generated using the GMT software package created by Pål Wessel and Walter Smith.

References

Andeweg, B., 2002. Cenozoic tectonic evolution of the Iberian Peninsula, causes and effects of changing stress fields. Unpublished PhD Thesis, Vrije Universiteit Amsterdam 178 pp.

Artyushkov, E.V., 1973. Stresses in the lithosphere caused by crustal thickness inhomogeneities. J. Geophys. Res. 78, 7675–7708.

Bada, G., Horvath, F., Cloetingh, S., Coblentz, D., Toth, T., 2001. Role of topography-induced gravitational stresses in basin inversion: the case study of the Pannonian basin. Tectonics 20, 343–363.

Balling, N., Svenningsen, L., Jacobsen, B.H., Kind, R., 2006. Seismological and gravity evidence for a crustal root beneath the highlands of Southern Norway and tectonic implications. In: Pascal, C., Lombaerts, F. (Eds.), 1st TopoNorge Workshop. Abstracts and proceedings of the Geological Society of Norway, vol. 1.

Bowin, C., 1991. The Earth's gravity field and plate tectonics. Tectonophysics 187, 69–89.

Boyd, F.R., 1989. Compositional distinction between oceanic and cratonic lithosphere. Earth Planet. Sci. Lett. 96, 15–26.

Boyd, F.R., McCallister, R.H., 1976. Densities of fertile and sterile garnet peridotites. Geophys. Res. Lett. 3, 509–512.

Boyd, F.R., Pearson, D.G., Mertzman, S.A., 1999. Spinel-facies peridotites from the Kaapvaal root. In: Gurney, J.J., et al. (Ed.), Proceedings of the VIIth International Kimberlite Conference, 1, pp. 40–48. Red Roof Design, Cape Town, South Africa.

Bott, M.H.P., 1991. Ridge push and associate plate interior stress in normal and hot spot regions. Tectonophysics 200, 17–32.

Brook, E.J., Nesje, A., Lehman, S.J., Raisbeck, G.M., Yiou, F., 1996. Cosmogenic nuclide exposure ages along a vertical transect in western Norway: implications for the height of the Fennoscandian ice sheet. Geology 24, 207–210.

Bungum, H., Alsaker, A., Kvamme, L.B., Hansen, R.A., 1991. Seismicity and seismotectonics of Norway and surrounding continental shelf areas. J. Geophys. Res. 96, 2249–2265.

Burov, E.B., Diament, M., 1995. The effective elastic thickness (T_e) of continental lithosphere: what does it really mean? J. Geophys. Res. 100, 3905–3927.

Calcagnile, G., 1982. The lithosphere–asthenosphere system in Fennoscandia. Tectonophysics 90, 19–35.

Carter, N.L., Tsenn, M.C., 1987. Flow properties of continental lithosphere. Tectonophysics 136, 27–33.

Christensen, N.J., Mooney, W.D., 1995. Seismic velocity structure and composition of the continental crust: a global view. J. Geophys. Res. 100, 9761–9788.

(33 authors)Cloetingh, S.A.P.L., et al., 2007. Topo-Europe: the geoscience of coupled deep Earth-surface processes. Glob. Planet. Change 58, 1–118.

Coblentz, D.D., Richardson, R., Sandiford, M., 1994. On the gravitational potential of the Earth's lithosphere. Tectonics 13, 929–945.

Dahlen, F.A., 1981. Isostasy and the ambient state of stress in the oceanic lithosphere. J. Geophys. Res. 86, 7801–7807.

Dehls, J.F., Olesen, O., Bungum, H., Hicks, E., Lindholm, C.D., Riis, F., 2000. Neotectonic map, Norway and adjacent areas 1:3 mill. Geological Survey of Norway, Trondheim.

Doré, A.G., Lundin, E.R., Kusznir, N., Pascal, C., 2008. Potential mechanisms for the genesis of Cenozoic domal structures on the NE Atlantic margin: pros, cons and some new ideas. In: Johnson, H., et al. (Ed.), The Nature and Origin of Compression in Passive Margins. Spec. Pub. Geol. Soc. London, vol. 306, pp. 1–26.

Fejerskov, M., Lindholm, C.D., 2000. Crustal stress in and around Norway; an evaluation of stress-generating mechanisms. In: Nøttvedt, A. (Ed.), Dynamics of the Norwegian Margin. Geological Society, London, Special Publications, vol. 167, pp. 451–467.

Fjeldskaar, W., 1997. Flexural rigidity of Fennoscandia inferred from the postglacial uplift. Tectonics 16, 596–608.

Fleitout, L., Froidevaux, C., 1982. Tectonics and topography for a lithosphere containing density heterogeneities. Tectonics 1, 21–56.

Ghosh, A., Holt, W.E., Flesch, L.M., Haines, A.J., 2006. Gravitational potential energy of the Tibetan Plateau and the forces driving the Indian plate. Geology 34, 321–324.

Goetze, C., Evans, B., 1979. Stress and temperature in the bending lithosphere as constrained by experimental rock dynamics. Geophys. J. R. Astron. Soc. 59, 463–478.

Gölke, M., Cloetingh, S., Coblentz, D., 1996. Finite-element modeling of stress patterns along the Mid-Norwegian continental margin, 62° to 68°N. Tectonophysics 266, 33–53.

Gregersen, S., 2006. Intraplate earthquakes in Scandinavia and Greenland, neotectonics or postglacial uplift? J. Ind. Geophys. Union 10, 25–30.

Grollimund, B., Zoback, M.D., 2000. Post glacial lithospheric flexure and induced stresses and pore pressure changes in the northern North Sea. Tectonophysics 327, 61–81.

Grollimund, B., Zoback, M.D., 2003. Impact of glacially induced stress changes on fault-seal integrity offshore Norway. AAPG Bull. 87, 493–506.

Heidbach, O., Tingay, M., Barth, A., Reinecker, J., Kurfess, D. and Müller, B., 2008. The 2008 release of the World Stress Map (available online at www.world-stress-map.org).

Hicks, E.C., Bungum, H., Lindholm, C.D., 2000. Stress inversion of earthquake focal mechanism solutions from onshore and offshore Norway. Norsk Geologisk Tidsskrift 80, 235–250.

Iaffaldano, G., Bunge, H.-P., Dixon, T.H., 2006. Feedback between mountain belt growth and plate convergence. Geology 34, 893–896.

Jaeger, J.C., Cook, N.G.W., 1969. Fundamentals of Rock Mechanics. Chapman and Hall, London. 515 pp.

James, D.E., Boyd, F.R., Schutt, D., Bell, D.R., Carlston, R.W., 2004. Xenolith constraints on seismic velocities in the upper mantle beneath southern Africa. Geochem. Geophys. Geosyst. 5, 1–32.

Jarosiński, M., Beekman, F., Bada, G., Cloetingh, S., 2006. Redistribution of recent collision push and ridge push in Central. Europe: insights from FEM modelling. Geophys. J. Int. 167, 860–880.

Jones, C.H., Unruh, J.R., Sonder, L.J., 1996. The role of gravitational potential energy in active deformation in the southwestern United states. Nature 381, 37–41.

Jordan, T.H., 1988. Structure and formation of the continental tectosphere. J. Petrol. 29, 11–37.

Kinck, J.J., Husebye, E.S., Larsson, F.R., 1993. The Moho depth distribution in Fennoscandia and the regional tectonic evolution from Archean to Permian times. Precambrian Res. 64, 23–51.

Lachenbruch, A.H., Morgan, P., 1990. Continental extension, magmatism and elevation; formal relations and rules of thumb. Tectonophysics 174, 39–62.

Lagerbäck, R., 1990. Late Quaternary faulting and paleoseismicity in northern Fennoscandia, with particular reference to the Lansjärv area, northern Sweden. Geologiska Föreningens i Stockholm Förhandlingar 112, 333–354.

Lemoine, F.G., Smith, D., Smith, R., Kunz, L., Pavlis, E., Pavlis, N., Klosko, S., Chinn, D., Torrence, M., Williamson, R., Cox, C., Rachlin, K., Wang, Y., Kenyon, S., Salman, R., Trimmer, R., Rapp, R., Nerem, S., 1996. EGM96, The NASA GSFC and NIMA Joint Geopotential Model. Proceedings of the International Symposium on Gravity, Geoid, and Marine Geodesy, Tokyo, Japan, September 30 –October 4.

Lindholm, C.D., Bungum, H., Bratli, R.K., Aadnoy, B.S., Dahl, N., Tørudbakken, B., Atakan, K., 1995. Crustal stress in the northern North Sea as inferred from borehole breakouts and earthquake focal mechanisms. Terra Nova 7, 51–59.

Lindholm, C., Bungum, H., Hicks, E., Villagran, M., 2000. Crustal stress and tectonics in Norwegian regions determined from earthquake focal mechanisms. In: Nøttvedt, A. (Ed.), Dynamics of the Norwegian margin. Geological Society, London, Special Publications, vol. 167, pp. 429–439.

McNutt, M., Diament, M., Kogan, M.G., 1988. Variations of elastic plate thickness at continental thrust belts. J. Geophys. Res. 93, 8825–8838.

Mosar, J., Lewis, G., Torsvik, T.H., 2002. North Atlantic sea-floor spreading rates: implications for the Tertiary development of inversion structures of the Norwegian–Greenland Sea. Journal of the Geological Society, London 159, 503–515.

Muir Wood, R., 2000. Deglaciation seismotectonics: a principal influence on intraplate seismogenesis at high latitudes. Quat. Sci. Rev. 19, 1399–1411.

Nesje, A., Dahl, S.O., Anda, E., Rye, N., 1988. Block fields in southern Norway: significance for the Late Weichselian ice sheet. Norsk Geologisk Tidsskrift 68, 149–169.

Olesen, O., 1988. The Stuoragurra Fault, evidence of neotectonics in the Precambrian of Finnmark, northern Norway. Norsk Geologisk Tidsskrift 68, 107–118.

Pascal, C., 2006. On the role of heat flow, lithosphere thickness and lithosphere density on gravitational potential stresses. Tectonophysics 425, 83–99.

Pascal, C., Cloetingh, S.A.P.L., Davies, G.R., 2004. Asymmetric lithosphere as the cause of rifting and magmatism in the Permo-Carboniferous Oslo Graben, in Permo-Carboniferous Rifting and Magmatism in Europe. In: Wilson, M., et al. (Ed.), Spec. Pub. Geol. Soc. London, vol. 223.

Pascal, C., Gabrielsen, R.H., 2001. Numerical modelling of Cenozoic stress patterns in the Mid Norwegian Margin and the northern North Sea. Tectonics 20, 585–599.

Pascal, C., Roberts, D., Gabrielsen, R.H., 2005. Quantification of neotectonic stress orientations and magnitudes from field observations in Finnmark, northern Norway. J. Struct. Geol. 27, 859–870.

Pérez-Gussinyé, M., Watts, A.B., 2005. The long-term strength of Europe and its implications for plate forming processes. Nature 436. doi:10.1038/nature03854.

Plomerová, J., Arvidsson, R., Babuška, V., Granet, M., Kulhanek, O., Poupinet, G., Šileny, J., 2001. An array study of lithospheric structure across the Protogine zone, Värmland, south-central Sweden — signs of a paleocontinental collision. Tectonophysics 332, 1–21.

Pollack, H.N., Hurter, S.J., Johnson, J.R., 1993. Heat loss from the Earth's interior: analysis of the global data set. Rev. Geophys. 31, 267–280.

Poudjom Djomani, Y.H., O'Reilly, S.Y., Griffin, W.L., Morgan, P., 2001. The density structure of subcontinental lithosphere through time. Earth Planet. Sci. Lett. 184, 605–621.

Roberts, D., Myrvang, A., 2004. Contemporary stress orientation features and horizontal stress in bedrock, Trøndelag, central Norway. NGU Bull. 442, 53–63.

Rohrman, M., van der Beek, P.A., van der Hilst, R.D., Reemst, P., 2002. Timing and mechanisms of North Atlantic Cenozoic Uplift: Evidence for mantle upwelling. In: A.G., J.A., Cartwright, Stoker, M.S., Turner, J.P., White, N. (Eds.), Exhumation of the North Atlantic Margin: Timing, Mechanisms and Implications for Petroleum Exploration. Geological Society of London, Special Publications, pp. 27–43.

Stein, S., Cloetingh, S., Sleep, N.H., Wortel, R., 1989. Passive margin earthquakes, stresses and rheology. In: Gregersen, S., Basham, P.W. (Eds.), Earthquakes at North-Atlantic Passive Margins; Neotectonics and Postglacial Rebound. NATO ASI Series, Series C: Mathematical and Physical Sciences, vol. 266. D. Reidel Publishing Company, Dordrecht-Boston, International, pp. 231–259.

Svenningsen, L., Balling, N., Jacobsen, B.H., Kind, R., Wylegalla, K., Schweitzer, J., 2007. Crustal root beneath the highlands of southern Norway resolved by teleseismic receiver functions. Geophys. J. Int. 170, 1129–1138.

ter Voorde, M., Færseth, R.B., Gabrielsen, R.H., Cloetingh, S.A.P.L., 2000. Repeated lithospheric extension in the northern Viking Graben: a coupled or a decoupled rheology? In: Nøttvedt, A., et al. (Ed.), Dynamics of the Norwegian Margin. Geol. Soc. London Spec. Publ., vol. 167, pp. 59–81.

Turcotte, D.L., Schubert, G., 2002. Geodynamics, 2nd ed. Cambridge University Press. 456 pp.

Watts, A.B., Bodine, J.H., Ribe, N.M., 1980. Observations of flexure and the geological evolution of the Pacific Ocean basin. Nature 283, 532–537.

Winguth, C., Mickelson, D.M., Larsen, E., Darter, J.R., Moeller, C.A., Stalsberg, K., 2005. Thickness evolution of the Scandinavian ice sheet during the Late Weichselian in Nordfjord, western Norway: evidence from ice-flow modeling. Boreas 34, 176–185.

Zoback, M.L., Mooney, W.D., 2003. Lithospheric buoyancy and continental intraplate stresses. Int. Geol. Rev. 45, 95–118.